

The Cluster Wind from Local Massive Star Clusters

Ian R. Stevens, Joanna M. Hartwell

School of Physics and Astronomy, University of Birmingham, Edgbaston, Birmingham B15 2TT
(E-mail: irs@star.sr.bham.ac.uk, jmh@star.sr.bham.ac.uk)

13 November 2018

ABSTRACT

Results of a study of the theoretically predicted and observed X-ray properties of local massive star clusters are presented, with a focus on understanding the mass and energy flow from these clusters into the ISM via a cluster wind. A simple theoretical model, based on the work of Chevalier & Clegg (1985), is used to predict the theoretical cluster properties, and these are compared to those obtained from recent *Chandra* observations. The model includes the effect of lower energy transfer efficiency and mass-loading. In spite of limited statistics, some general trends are indicated; the observed temperature of the diffuse X-ray emission is lower than that predicted from the stellar mass and energy input rates, but the predicted scaling of X-ray luminosity with cluster parameters is seen. The implications of these results are discussed.

Key words: hydrodynamics: shock waves; open clusters and associations; stars: winds, outflows

1 INTRODUCTION

Super Star Clusters are dense clusters of young massive stars, first identified in NGC 1275 by Holtzman et al. (1992) using the *Hubble Space Telescope* (HST), and subsequently in a wide range of star-forming galaxies, such as merging systems (NGC 4038/4039; Whitmore & Schweizer 1995), dwarf galaxies (Henize 2-10; Johnson et al. 2000), classical starbursts (M82; Gallagher & Smith 1999) amongst many other systems (see Whitmore 2000 for a review). These extragalactic star clusters can contain many thousands of very young, energetic stars, and have stellar densities far greater than those seen in normal OB associations. The values quoted by Whitmore (2000) indicate ages for these star clusters of typically 1 – 10 Myr, radii typically in the range of $\sim 1 - 6$ pc, total masses of stars in the cluster in the range $10^3 - 10^6 M_{\odot}$, with the central stellar densities reaching up to $\sim 10^5 M_{\odot} \text{ pc}^3$. It is clear that in many galaxies a substantial fraction of the ongoing star-formation (and hence mass/energy injection into the ISM) is occurring in SSCs (Origlia et al. 2001). The Galactic (or local analogues) of these extragalactic SSCs are objects such as NGC 3603, R136 in 30 Doradus and the Arches cluster near the Galactic Centre (see Figer, McLean & Morris 1999b).

The component stars of an SSC are believed to be roughly coeval, and when the cluster is very young the massive stars in the cluster will have strong stellar winds which will combine to produce an outflow from the cluster, which is referred to as the cluster wind. As the cluster ages mass and energy input from supernova explosions will begin to

dominate (cf. Leitherer & Heckman 1995). In many starburst galaxies, where a large number of SSCs are seen, this cluster wind will be an important contributor to energising the interstellar medium and possibly driving a hot superwind or outflow, such as those seen in M82 or NGC 253 (Lehnert, Heckman & Weaver 1999; Strickland et al. 2002). The efficiency with which stellar kinetic energy (from both stellar winds and supernovae) is converted into thermal energy within the cluster, which in turn can drive an outflow, is an important and very difficult parameter to determine. In the literature, several different values or prescriptions for the thermalization efficiency have been used, often encapsulated in a parameter η , which represents the fraction of the kinetic energy of stars and supernova in the cluster that is thermalized. The fraction of the kinetic energy that is not thermalized is assumed to be lost to the system, primarily via radiative losses. As we shall see radiative losses at X-ray energies are likely to be very small, however, at UV and IR energies radiative losses are likely to be much larger. In fact, inhomogeneities in the complex flow within the cluster could easily lead to the formation of denser regions that could contribute to radiating energy away from the system.

In the literature, Strickland & Stevens (2000) argued for very efficient thermalization ($\eta \sim 1$; see also Chevalier & Clegg 1985), whereas Bradamante, Matteucci & D’Ercole (1998) argued for a much lower thermalization efficiency of a few per cent. Other, more complex, prescriptions of η have also been proposed. For instance, Recchi, Matteucci & D’Ercole (2001) use a model with η being very low in the early evolution of a cluster, but as material is evacu-

arXiv:astro-ph/0301038v1 3 Jan 2003

ated by the cluster wind to create a low density region the thermalization efficiency rises to close to unity. In relation to LMC superbubbles, Oey (1996) noted that the bubble dynamics implied a relatively low thermalization efficiency (or put another way that there was less power driving the bubbles than implied by the stellar populations within the bubbles, see also Chu & Mac Low for a discussion of the X-ray properties of superbubbles). It would clearly be very useful to have more direct observational constraints on this process.

Understanding the mass and energy loss processes from distant SSCs via the hot cluster wind can best be done at X-ray energies. However, because of their distance and the high stellar density, even *Chandra* has insufficient resolution to see what is going on in and around these systems, and resolve the diffuse emission from point source emission from stars in the cluster. However, local lower-mass analogues of these SSCs in our Galaxy or Local Group can be used to study the mass and energy loss processes from stellar clusters. By studying the diffuse X-ray properties of star clusters and the stellar energy injection rate from stellar populations in the cluster it should be possible to constrain the efficiency with which the clusters can convert kinetic energy to thermal energy. Although not perfect analogues, the values determined could have far-reaching consequences, not just for the understanding of the processes within the star clusters, but also for the energy emission from larger structures such as starburst galaxies, where many SSCs are present.

It is also worth making the point that while the mass and energy injection rate from massive stars via their stellar winds can be estimated to a reasonable degree of accuracy, the same is less true for supernova. For instance, it is worth noting that the type II_n supernova SN1988Z is believed to have radiated $\sim 10^{52}$ erg in its early evolution (Aretxaga et al. 1999), see also Chevalier & Fransson 2001), which is rather more than the usually assumed values for the total energy injection from a SN. Consequently, looking at very young clusters, where SN injection does not dominate, has considerably more promise.

In this paper the theory of cluster winds is developed, particularly as it relates to X-ray emission from clusters (§ 2), and it is then applied to results from *Chandra* observations of nearby SSCs or smaller stellar clusters (§ 3). The results are discussed in § 4 and summarised in § 5.

2 THE X-RAY EMISSION FROM A CLUSTER WIND

When massive stars with strong winds are in close proximity, such as in a stellar cluster, the winds collide both with each other and with the surrounding ISM, filling the surrounding volume with hot shocked gas. Eventually all of the available volume is filled and the hot gas escapes beyond the boundaries of the cluster. The development of such a cluster wind has been numerically modelled by Cantó, Raga & Rodríguez (2000) in a simulation carried out assuming a spherical cluster consisting of ~ 30 stars (see also Ozernoy, Genzel & Usov 1997; Raga et al. 2001).

The wind from a stellar cluster can also be described using the Chevalier & Clegg (1985) model originally used to

describe outflows from starburst galaxies. The contrast between these models is that Cantó et al. (2000) also used hydrodynamic calculations with mass and energy input from discrete stars within the cluster, whereas the Chevalier & Clegg (1985) model assumed mass and energy injection uniformly throughout the starburst region. The dense star clusters considered here do not have a uniform distribution of stars and tend to be centrally concentrated, and mass and energy injection will tend to follow the stellar distribution. However, Cantó et al. (2000), who did include a non-uniform stellar distribution showed that their numerical simulations generally reproduce the results of the Chevalier & Clegg type model, and the formulation of Chevalier & Clegg (1985) is adopted here. One important difference between the Cantó et al. (2000) and Chevalier & Clegg (1985) models is that the Cantó et al. (2000) have a much greater range of temperatures (and densities inside the cluster core).

If mass and energy from stars is being injected via stellar winds into the volume of a stellar cluster of core radius R_c then Chevalier & Clegg (1985) showed that the solution for the outflow from this region can be written as

$$\left(\frac{3\gamma + 1/\mathcal{M}^2}{1 + 3\gamma}\right)^{-\frac{(3\gamma+1)}{(5\gamma+1)}} \left(\frac{\gamma - 1 + 2/\mathcal{M}^2}{1 + \gamma}\right)^{\frac{(\gamma+1)}{2(5\gamma+1)}} = \frac{r}{R_c} \quad (1)$$

for $r < R_c$ and

$$\mathcal{M}^{2/(\gamma-1)} \left(\frac{\gamma - 1 + 2/\mathcal{M}^2}{1 + \gamma}\right)^{((\gamma+1)/2(\gamma-1))} = \left(\frac{r}{R_c}\right)^2 \quad (2)$$

for $r > R_c$, where \mathcal{M} is the Mach number of the flow, γ is the adiabatic index (with $\gamma = 5/3$ assumed hereafter), R_c the radius of the star cluster and r is the radius from the center of star cluster. From these equations and the mass and energy injection rates, the velocity $v(r)$, temperature $T(r)$ and mass density $\rho(r)$ can be determined. The technique to do so involves solving eqn. 1 or eqn. 2 as appropriate, for the Mach number at each radius, using the Newton-Raphson method. From the Mach number, and using the integrated forms of the mass and energy equations, the other variables can be determined (see Chevalier & Clegg 1985 for more details). Solar abundances and fully ionized material with a mean mass per particle of $\bar{\mu} = 10^{-24}$ gm are also assumed.

It is worth noting that the conditions in the central regions of the cluster are a good indicator of the recent history of the cluster. The flow time within the cluster is short, typically a few 10^3 yr, whereas the characteristic timescale of the larger scale bubble being blown by the cluster is much longer (i.e. of order the age of the cluster). This means that the current X-ray properties should give a better handle on the transfer efficiency of stellar wind energy to the cluster wind.

2.1 The Stellar Mass and Energy Injection Rate

For the young star clusters under consideration here the energy injection is dominated by stellar winds, especially those of the massive OB and Wolf-Rayet (WR) stars, and we assume that no supernovae have as yet exploded and contributed to the cluster wind. At later epochs supernovae begin to dominate the energy injection (Leitherer & Heckman 1995).

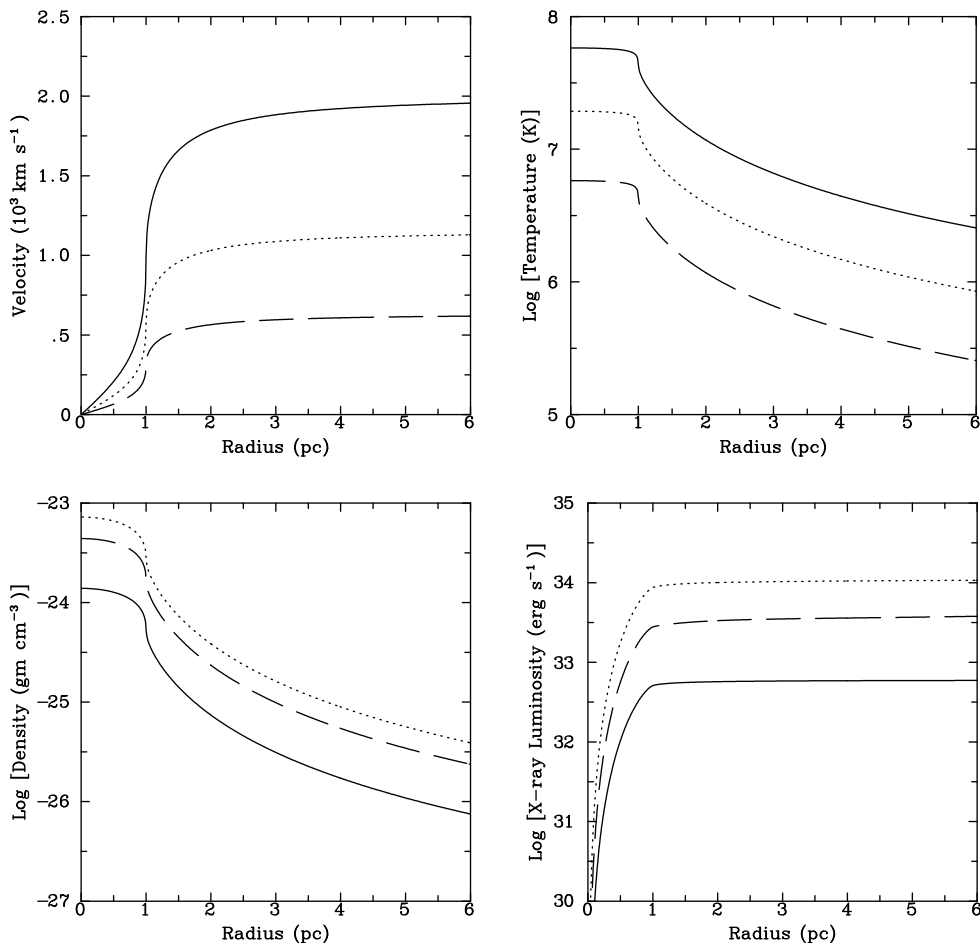


Figure 1. The radial structure for the cluster wind, as calculated from the Chevalier & Clegg (1985) model (see text for details). Shown are the radial profiles for the wind velocity (top left panel), gas temperature (top right), density (bottom left) and the cumulative X-ray luminosity (bottom right). The standard model (solid line) is for a star cluster with a stellar mass injection rate of $\dot{M}_* = 10^{-4} M_\odot \text{ yr}^{-1}$, $\bar{V}_* = 2000 \text{ km s}^{-1}$, $\eta = 1$ and no additional mass-loss ($\dot{M}_{\text{cold}} = 0$). The second model is identical, except with $\eta = 0.1$ (dashed line), and the third model (dotted line) has $\eta = 1$ and $\dot{M}_{\text{cold}} = 2 \times 10^{-4} M_\odot \text{ yr}^{-1}$.

In principal, from the current observed massive star population in the clusters, the mass and energy injection rate from the stellar winds of these stars can be estimated, and this is the procedure we adopt. However, as discussed elsewhere, there are some significant uncertainties in the determination of these values, related to uncertainties in understanding the structure and evolution of massive stars.

The bulk of the mass and energy injection is assumed to happen within a cluster core radius R_c . If the cluster contains N_* stars, each star with a mass-loss rate of \dot{M}_i and wind terminal velocity V_i with $i = 1 \dots N_*$ then the total stellar wind mass injection rate, \dot{M}_* , is

$$\dot{M}_* = \sum_i^{N_*} \dot{M}_i \quad (3)$$

and the total kinetic energy injection rate is

$$\dot{E}_* = \sum_i^{N_*} \frac{1}{2} \dot{M}_i V_i^2. \quad (4)$$

A mean weighted terminal velocity for the stars in the clusters is defined such that

$$\bar{V}_* = \left(\frac{\sum_i^{N_*} \dot{M}_i V_i^2}{\dot{M}_*} \right)^{1/2} \quad (5)$$

For some of the stellar clusters discussed in the next section the individual mass-loss rates and terminal velocities can be determined, and for those systems where there is insufficient observational evidence stellar evolution models, such as the *Starcburst99* code (Leitherer et al. 1999) can be used.

Some qualifications should be made here. The method used for estimating the mass-loss rates and terminal velocities of the cluster stars rests on our current best understanding of the mass-loss parameters of massive stars. There remain significant deficiencies in our knowledge of the structure and evolution of massive stars and their winds. For instance, the *Starcburst99* code only assumes a population of single stars and binary evolution could make a difference to the mass-loss rates and terminal velocity. Indeed, it is known that the characteristics of the winds of massive stars

evolve with time, and this snapshot could be missing important early phases of evolution when the winds were much stronger. In spite of these qualifications we shall use current best estimates and proceed accordingly.

In a cluster although the optically visible stars (and their winds) will likely dominate the energy injection, these stars will not necessarily be the only sources of mass. Protostars (or other optically obscured objects) will also contribute mass as material is ablated off them by the cluster wind or through radiation. Examples of such objects may be the ProPlyDs which have been seen in NGC 3603 and elsewhere (for instance, Brandner et al. 2000; Mücke et al. 2002). This cold mass being injected into the cluster wind can be accounted for by a term \dot{M}_{cold} , so that the total mass-loss rate into the cluster is

$$\dot{M}_{tot} = \dot{M}_* + \dot{M}_{cold} \quad (6)$$

This process can be considered as a mass-loading process (see Hartquist et al. 1997 and references therein).

As discussed in the introduction, to account for the effects of radiative losses in the conversion of stellar wind energy into the cluster wind, we can introduce a parameter that we term the ‘‘thermalization efficiency’’ parameter η , such that the energy available to drive the cluster wind is $E_{th} = \eta E_*$, so that

$$\dot{E}_{th} = \eta \sum_i^{N_*} \frac{1}{2} \dot{M}_i V_i^2 = \frac{\eta}{2} \dot{M}_* \bar{V}_*^2 \quad (7)$$

and allow η to vary between 0 and 1. This parameter allows for radiative losses. The energy radiated at X-ray energies is unlikely to be a major loss mechanism, but UV radiation, particularly from interfaces between hot and cold gas, may be a bigger contributor, as could IR radiation. As discussed by Recchi et al. (2001) we might expect this parameter to be relatively small in the early stages of cluster evolution, but to increase at later times. For simplicity, in these simulations η is assumed constant. The result of allowing η to be less than unity and additional ‘‘cold’’ mass-injection will be to reduce the terminal cluster wind velocity below \bar{V}_* . This in turn increases the density and often leads to an enhanced X-ray luminosity.

The assumption of a constant thermalization efficiency is also highly simplistic. Not only is the value likely to vary as a function of time, as the cluster wind evolves, it is also likely to vary as a function of location within the cluster, with a different thermalization efficiency in the denser inner regions to that in the more diffuse outer regions. Given the lack of detailed information as to how η might vary, we shall treat it as a constant. So, subject to this recognition that this is a highly simplified treatment of a very complex problem we shall proceed.

2.2 The Cluster X-ray Luminosity

Observationally, at X-ray wavelengths, a young stellar cluster will have both point source emission associated with individual stars, such as from colliding winds in massive binaries, intrinsic emission from single early-type stars, emission associated with SNRs, X-ray binaries or pre-main sequence stars, and diffuse emission (due to the cluster wind). Here we concentrate only on the diffuse X-ray emission, and only from

younger clusters where we would not expect to see emission from SNRs and X-ray binaries. In the data presented later, the point sources have been removed from the X-ray data to leave only the diffuse emission. It is however possible that unresolved point sources, particularly from lower luminosity pre-main sequence (PMS) stars, will contaminate the diffuse emission. We will discuss this point more later.

For a given model, the broad-band X-ray luminosity of the cluster will be given by

$$L_X = \int_0^{R_c} 4\pi r^2 n_e n_i \Lambda(T) dr \quad (8)$$

where $\Lambda(T)$ is the emissivity of gas at a temperature T , and n_e and n_i are the electron and ion number density respectively. Given the solution for $\rho(r)$, $v(r)$ etc, eqn. 8 can be evaluated to derive the total X-ray luminosity (over a wide waveband) of the cluster. A more detailed analysis could calculate the luminosity in specific wavebands. However, the majority of the emission will fall in the *Chandra* waveband and we will not complicate matters further.

In Fig. 1 the radial variation of the velocity and temperature for a stellar cluster are shown, where the total stellar mass-loss rate is $10^{-4} M_\odot \text{ yr}^{-1}$ and $\bar{V}_* = 2000 \text{ km s}^{-1}$ and the cluster core radius is 1pc. These values are similar to those of the clusters discussed in this paper. In this model the central temperature is $5.8 \times 10^7 \text{ K}$, the central ion number density is 0.67 cm^{-3} , and the X-ray luminosity of the region within a radius R_c is $L_X = 5.1 \times 10^{32} \text{ erg s}^{-1}$. Importantly for our purposes, the cluster itself dominates the X-ray emission and the volume outside R_c contributes only 15 per cent of the total X-ray luminosity. The reason for this is the sharp fall off in density (and temperature) outside the cluster, which more than compensates for the increasing volume of the emission region. For a simple analysis such as presented here this level of accuracy is sufficient.

The central temperature of the cluster wind (T_0) in this model is given by

$$\left(\frac{T_0}{\text{K}}\right) = 1.45 \times 10^7 \left(\frac{\bar{V}_*}{1000 \text{ km s}^{-1}}\right)^2. \quad (9)$$

Note that the slightly different numerical constant as compared to Cantó et al. (2000) is due to slightly different assumptions as to the mean mass per particle.

From the radial solution the emission weighted temperature for the cluster region (T_{cl}) can also be calculated, which will be somewhat lower than the central temperature. For instance, for the standard model with $\bar{V}_* = 2000 \text{ km s}^{-1}$, the emission weighted temperature is $T_{cl} = 5.1 \times 10^7 \text{ K}$.

Results of models illustrating the effect of η and mass-loading on the expected cluster temperature are shown in Fig. 2, and show that, not surprisingly, both mass-loading and $\eta < 1$ lead to lower cluster temperatures, but also, often, higher X-ray luminosities.

2.3 X-ray Luminosity Scaling Relations

Given that the gas temperature within the cluster is comparatively constant (see Fig. 1) and hot (for $\bar{V}_* \geq 1000 \text{ km s}^{-1}$ the temperatures are $> 10^7 \text{ K}$, so that the bremsstrahlung region of the cooling curve is appropriate, i.e. $\Lambda(T) \propto T^{1/2}$)

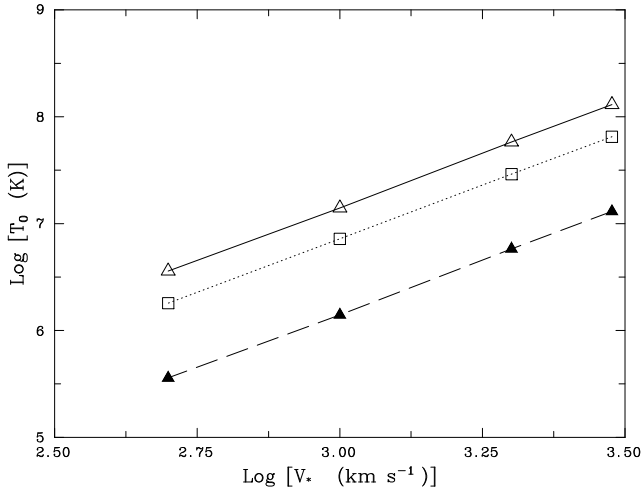


Figure 2. The variation of the expected X-ray temperature of the cluster core versus the wind velocity of the stellar component. Shown are model results for the cluster central temperature and cluster luminosity for varying η and the contribution of cold gas. The standard cluster model has $\dot{M}_* = 10^{-4} M_\odot \text{ yr}^{-1}$ and $R_c = 1 \text{ pc}$. The models represented by open triangles and marked with a solid line are for $\eta = 1$ and $\bar{V}_* = 500, 1000, 2000$ and 3000 km s^{-1} . The models represented by filled triangles and marked with a dashed line are the same models except with $\eta = 0.1$. The models represented by open squares and marked with a dotted line are the same models except with $\dot{M}_{cold} = \dot{M}_*$.

the following simple scaling relationships for the X-ray luminosity of clusters can be derived (ignoring for the time being the effects of $\eta < 1$ and mass-loading).

The gas density within the cluster, $n \propto \dot{M}_*/(R_c^2 \bar{V}_*)$, so that if we define a cluster wind scaling parameter X_{cl} such that

$$X_{cl} = \frac{\dot{M}_*^2}{R_c \bar{V}_*} \quad (10)$$

then from eqn. (8) $L_X \propto X_{cl}$. We shall calculate X_{cl} using the natural units, that is \dot{M} in $M_\odot \text{ yr}^{-1}$, R_c in pc and \bar{V}_* in km s^{-1} , so that for a model with $\dot{M}_* = 10^{-4} M_\odot \text{ yr}^{-1}$, $\bar{V}_* = 2000 \text{ km s}^{-1}$ and $R_c = 1 \text{ pc}$, then $X_{cl} = 5 \times 10^{-12}$.

At smaller velocities the deviations from the $T^{1/2}$ scaling for the cooling curve will alter things. For temperatures in the range of $10^{6.2} \leq T \leq 10^{6.5} \text{ K}$, then roughly $\Lambda(T) \propto T^{-0.6}$ and the corresponding expression for the variation of the X-ray luminosity is

$$L_X \propto \frac{\dot{M}_*^2}{R_c \bar{V}_*^{3.2}}. \quad (11)$$

The scaling effect of variation in η on the cluster properties can also be derived. A reduction in η effectively reduces the amount of thermal energy available to the cluster as a whole. For the same amount of mass-loss this will reduce the temperature, with $T_{cl} \propto \eta$, but also reduce the velocity of the cluster wind and increase the density.

For the bremsstrahlung dominant case ($\Lambda(T) \propto T^{1/2}$), the density $n \propto \dot{M}/(R_c^2 \bar{V}_*)$ and $\bar{V}_*^2 \propto \eta$, so that here $L_X \propto \eta^{-0.5}$. In the case of $\Lambda(T) \propto T^{-0.6}$, then $L_X \propto \eta^{-1.6}$. Somewhat counter-intuitively then, a reduction in η leads to a rise in X-ray luminosity, due to the dominant effect of the

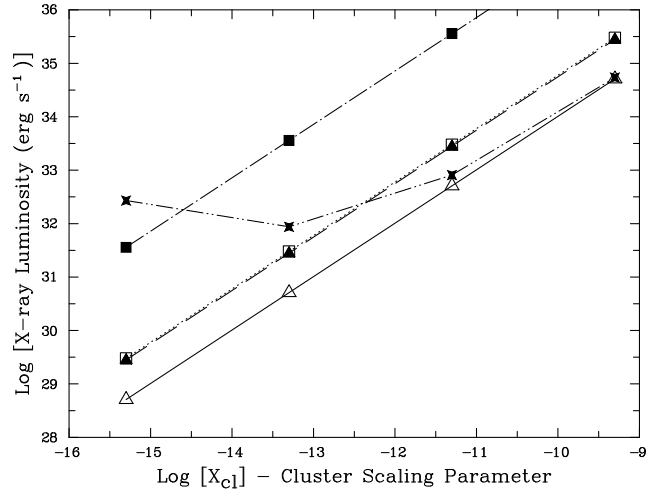


Figure 3. The theoretical cluster X-ray luminosity versus the cluster wind scaling parameter $X_{cl} = \dot{M}^2/(R_c \bar{V}_*)$. Results are shown for several different sets of models. The cluster radius is always 1 pc and $\bar{V}_* = 2000 \text{ km s}^{-1}$. The open triangles (and solid line) are for the standard models, which have no mass injection ($\dot{M}_{cold} = 0$) and $\eta = 1$, and stellar mass-loss rates of $\dot{M}_* = 10^{-6}, 10^{-5}, 10^{-4}$ and $10^{-3} M_\odot \text{ yr}^{-1}$. The filled triangles (dashed line) have the same parameters except $\eta = 0.1$. The open squares (dashed line) have $\eta = 1$ and $\dot{M}_{cold} = \dot{M}_*$ (and have very similar results to the previous models). The filled squares (dot-dashed line) have $\eta = 1$ and $\dot{M}_{cold} = 10\dot{M}_*$. The crosses (dot-dot-dashed line) have $\eta = 1$ and $\dot{M}_{cold} = 2 \times 10^{-5} M_\odot \text{ yr}^{-1}$.

increasing density. Of course, for $\eta \ll 1$ the emission will not be at X-ray energies and L_X will decrease. Results for the variation of the cluster X-ray luminosity versus this cluster scaling parameter are shown in Fig. 3, where models for a range of cluster wind scaling parameters X_{cl} are shown.

The effect of mass-loading is similar to the effect of lower values of η – both lead to a drop in the average available energy per particle. This is reflected in that models with $\eta = 0.1$ have almost identical results to a model with $\dot{M}_{cold} = \dot{M}_*$. Mass-loading leads to a decrease in temperature and an increase in density. Model results are also shown in Fig. 3. Of note is that the fact that we get a very different relationship between L_X and X_{cl} when the mass-loading injection is constant rather than a constant multiple of \dot{M}_* .

Disentangling the combined action of lower values of η and mass-loading in an individual cluster may be difficult, but in a statistical sample the relative influence of both effects may be apparent in star cluster X-ray luminosity–temperature plots. This is illustrated in Fig. 4, where for these simple models, different slopes in the cluster X-ray luminosity–temperature relationship are found when the effects of η and mass-loading are isolated and varied in a systematic manner. Whether in reality the two effects can be separated so cleanly is unclear. These models have also assumed a single cluster core radius. More realistic models, with a range of parameters will show more scatter.

Table 1. The observed and predicted properties of the cluster wind from the 5 star clusters under consideration. The values for \dot{M} and \bar{V}_* are obtained using eqns. 3 and 5 and are described more in the text. The predicted temperature, kT_0 , is calculated using eqn. 9. The expression for the cluster wind scaling parameter, X_{cl} , is given by eqn. 10. The sources for observed values for L_X and kT_X for each cluster are described in the text too.

Cluster	Predicted Values					Observed values	
	\dot{M}_* ($M_\odot \text{ yr}^{-1}$)	\bar{V}_* (km s^{-1})	R_c (pc)	X_{cl}	Predicted kT_0 (keV)	Observed kT_X (keV)	L_X (erg s^{-1})
NGC 3603	2.3×10^{-4}	2844	2.8	6.6×10^{-12}	10.1	3.7	2.2×10^{34}
R136	2.6×10^{-4}	2110	2.0	1.6×10^{-11}	5.6	2.1	5.5×10^{34}
NGC 346	1.7×10^{-5}	2282	2.0	6.4×10^{-14}	6.5	1.0	1.5×10^{34}
Rosette	2.5×10^{-6}	2173	4.6	6.3×10^{-16}	5.9	0.6	8.0×10^{32}
Arches	7.3×10^{-4}	2810	0.2	9.5×10^{-10}	9.9	0.8,6.4	5.0×10^{35}

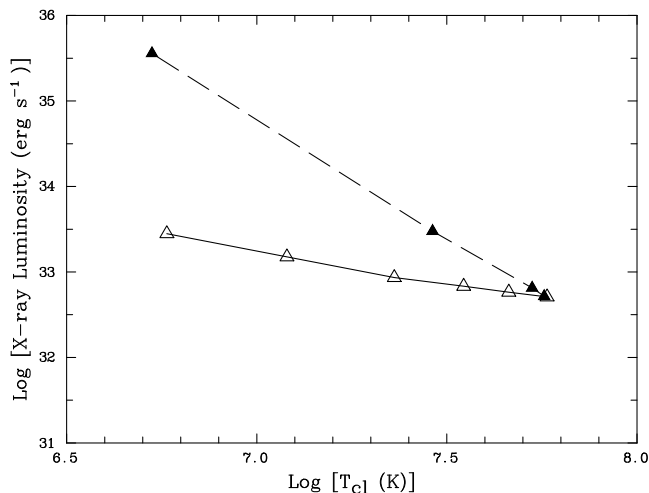


Figure 4. The theoretical stellar cluster X-ray luminosity-temperature relationship. Shown are model results for the mean cluster temperature and cluster luminosity for varying η and the contribution of cold gas. The standard cluster model has $\dot{M}_* = 10^{-4} M_\odot \text{ yr}^{-1}$, $\bar{V}_* = 2000 \text{ km s}^{-1}$ and $R_c = 1 \text{ pc}$. The models represented by open triangles and marked with a solid line are for varying η , with models with $\eta = 1.0, 0.8, 0.6, 0.4, 0.2$ and 0.1 , with decreasing temperature corresponding to decreasing η . The models represented by filled triangles and marked with a dashed line are for variations with the amount of cold material injected \dot{M}_{cold} and have $\eta = 1.0$. The model results are for $\dot{M}_{cold} = 10^{-6}, 10^{-5}, 10^{-4}$ and $10^{-3} M_\odot \text{ yr}^{-1}$, with decreasing temperature corresponding to increasing \dot{M}_{cold} .

3 THE SAMPLE OF NEARBY STAR CLUSTERS

SSCs and other compact star clusters are relatively small objects with a typical size of a few pc, so even with the arcsecond resolution of *Chandra* only those that are nearby can be studied in any detail. In this study *Chandra* data for R136, NGC 3603, NGC 346, the Rosette Nebula and the Arches cluster are used. The definition of an SSC is rather vague and certainly the Rosette Nebula does not qualify. However, although it is a much smaller cluster the physics should be the same and so it is included. In this section we describe both the relevant properties of the stellar components of the cluster and the diffuse X-ray properties of the

X-ray emission as seen with the *Chandra* satellite. In some cases results from the literature are used, while in others an analysis of the data has been performed.

3.1 NGC 3603

NGC 3603 is the most massive visible HII region in our galaxy, and is commonly regarded as a Galactic analogue for extragalactic SSCs. It contains a very dense concentration of stars of ages of $\sim 2 - 3 \text{ Myr}$, including 3 WR stars in its core. In many ways it is similar to R136 in 30 Dor but without the surrounding cluster halo (Moffat et al. 1994). We assume a distance of 7 kpc.

The characteristics of the massive stars in NGC 3603 have been studied by Crowther & Dessart (1998), and using this data and Kudritzki & Puls (2000), the mass-loss rates and terminal velocity data for 44 stars within 2.8pc of the centre of the cluster have been tabulated. These stars will dominate the stellar mass and energy loss into the cluster. Based on these results, the total stellar mass-loss rate for NGC 3603 is estimated as $\dot{M}_* = 2.3 \times 10^{-4} M_\odot \text{ yr}^{-1}$ and the mean weighted terminal velocity as $\bar{V}_* = 2844 \text{ km s}^{-1}$. The cluster core radius is taken to be 2.8pc (Moffat et al. 1994).

Results from a 50ksec ACIS-I *Chandra* observation of NGC 3603 have already been presented in Moffat et al. (2002), and these data show strong evidence of a diffuse thermal component, probably associated with a cluster wind. To determine the spectral characteristics of the diffuse emission, point sources are excluded and the diffuse spectrum extracted. The spectrum has been fitted with an absorbed *mekal* model (*wabs*mekal*), with $N_H = 0.67 \times 10^{22} \text{ cm}^{-2}$, $kT_X = 3.7 \text{ keV}$, and the absorption corrected luminosity is $L_X = 2.2 \times 10^{34} \text{ erg s}^{-1}$ (see Table 1).

3.2 R136 in 30 Doradus

R136 is the central object of 30 Doradus in the LMC, and is regarded as the closest example of an SSC, and we assume a distance of 50 kpc (cf. Feigelson 2001). The spectral types and mass-loss rates of 39 stars in R136 were obtained from a study by Crowther & Dessart (1998), and the corresponding wind velocities from Kudritzki & Puls (2000). The cluster mass-loss rate is estimated to be $\dot{M}_* = 2.6 \times 10^{-4} M_\odot \text{ yr}^{-1}$ and the mean weighted terminal velocity as $\bar{V}_* = 2110 \text{ km s}^{-1}$. The cluster core radius is assumed to be 2pc (Crowther & Dessart 1998).

The X-ray data of R136 was obtained from the *Chandra* archive and consists of a 28ksec ACIS-I observation of 30 Doradus. The point sources within a region of radius $16''$ centred on the cluster were removed as for NGC 3603, and a spectrum was extracted from the remaining emission, and fitted again using an absorbed *mekal* model. The best fit spectrum to this emission

was an absorbed *mekal* model, with $N_H = 0.42 \times 10^{22} \text{ cm}^{-2}$, $kT_X = 2.1 \text{ keV}$, and absorption corrected $L_X = 5.5 \times 10^{34} \text{ erg s}^{-1}$ (see Table 1).

3.3 NGC 346

NGC 346 is the largest star formation region of the SMC, and contains the majority of the O stars in the SMC (Massey, Parker & Garmany 1989). We assume a distance of 59 kpc (Mathewson, Ford & Visvanathan 1986). The spectral types and magnitudes of the stars in NGC 346 were obtained from Massey et al. (1989). Using a reddening correction of $E(B - V) = 0.14$, mass-loss rates were calculated from the expression in Howarth & Prinja (1989), accounting for the effects of lower metallicity on stellar mass-loss rates, with $\dot{M}(Z) \propto (Z/Z_\odot)^{0.5}$ (cf Kudritzki & Puls 2000 and using a value for the SMC metallicity of $Z_\odot/5$). The cluster mass-loss rate for NGC 346 is estimated to be $\dot{M}_* = 1.7 \times 10^{-5} M_\odot \text{ yr}^{-1}$ and the mean weighted terminal velocity as $\bar{V}_* = 2282 \text{ km s}^{-1}$. The cluster core radius is taken to be 2 pc (Massey et al. 1989).

Chandra observed NGC 346 for a total of 100 ksec in May 2001. The cluster lies close to a chip gap of the ACIS-I instrument, but diffuse emission from the cluster is still detected. A more detailed analysis of the *Chandra* data of the NGC 346 region can be found in Nazé et al. (2002a; 2002b). The extracted spectrum was best fit with an absorbed *mekal* model, with $N_H = 0.42 \times 10^{22} \text{ cm}^{-2}$, $kT_X = 1.0 \text{ keV}$, and $L_X = 1.5 \times 10^{34} \text{ erg s}^{-1}$ (absorption corrected, see Table 1).

3.4 The Rosette Nebula, NGC 2237

The Rosette Nebula (NGC 2237) contains an open cluster, NGC 2244, and is one of the more massive diffuse nebulae. It is situated at a distance of 1.5 kpc (Gregorio-Hetem et al. 1998). The cluster wind parameters of the Rosette Nebula were calculated using the properties of the 26 O, B and A stars lying within 4.6 pc of the cluster centre, which corresponds to the rough extent of the X-ray emission.

Spectral types were obtained from *SIMBAD*, and the corresponding wind velocities from Kudritzki & Puls (2000). Mass-loss rates were evaluated using the relationship of Howarth & Prinja (1989), assuming $E(B - V) = 0.49$ (Massey, Johnson, DeGioia-Eastwood 1995). The resulting values for the Rosette Nebula are $\dot{M}_* = 2.5 \times 10^{-6} M_\odot \text{ yr}^{-1}$ and $\bar{V}_* = 2173 \text{ km s}^{-1}$. The cluster core radius is assumed to be 4.6 pc (see above).

Chandra observations of this region found a large number of point sources. On subtraction of these point sources, a weak diffuse component was discovered (see Montmerle et al. 2002; Townsley et al. 2002, in preparation). Fitting this with an absorbed Raymond-Smith model, the best fit parameters for the diffuse emission were $N_H = 7 \times 10^{21} \text{ cm}^{-2}$, $kT_X = 0.6 \text{ keV}$ and the absorption corrected luminosity was $L_X = 8 \times 10^{32} \text{ erg s}^{-1}$ in the 0.5 – 2 keV waveband.

3.5 The Arches Cluster

The Arches cluster is located at a projected distance of ~ 50 pc from the Galactic centre (Cotera et al. 1996; Portegies-Zwart 2001), and contains ~ 120 stars which have masses greater than $20 M_\odot$ (Serabyn, Shupe & Figer 1998). It is one of the densest star clusters known in the local group. Blum et al. (2001) have presented a $2 \mu\text{m}$ study of the stellar population of the Arches cluster, and inferred an age for the cluster of between 2 and 4.5 Myr. We

assume that the cluster core radius is 0.2 pc and that the cluster is at a distance of 8 kpc (Figer et al. 1999b).

Due to the lack of comprehensive data on the stars in the Arches cluster, we have adopted the simpler approach of calculating \dot{M}_* and \bar{V}_* using the *Starburst99* models¹. Based on the results of Figer et al. (1999a), for the Arches cluster we assume a top-heavy IMF (with $\alpha = 1.6$), solar abundances, high mass-loss stellar evolution tracks and a total stellar mass of $1.1 \times 10^4 M_\odot$ (for stars in the mass range 1 – $100 M_\odot$), and the appropriate values are taken for values in the range $t \sim 2 - 4.5$ Myr. For times > 3.5 Myr mass and energy injection from SN begin to play a role. For the Arches cluster, in this time span the derived values of the mean weighted terminal velocity are in the range $\bar{V}_* = 1800 - 2810 \text{ km s}^{-1}$, and the total stellar mass-loss is in the range $\dot{M}_* = (2.0 - 9.5) \times 10^{-4} M_\odot \text{ yr}^{-1}$. The corresponding large range in the cluster wind parameter is $X_{cl} = (0.85 - 25.0) \times 10^{-10}$.

From the *Starburst99* simulations it is interesting to note that the value of $\bar{V}_* \geq 1500 \text{ km s}^{-1}$ for all times of relevance to young clusters. In the *Starburst99* models only single stars are included and the energy injection rate from SN tails off at $t \sim 35$ Myr (in this model). In models including binaries, mass and energy injection from SN will continue to longer times due to the processes of mass transfer and binary evolution.

For convenience, we will adopt the values at a time of 4 Myr for the Arches cluster, with $\bar{V}_* = 2810 \text{ km s}^{-1}$, and $\dot{M}_* = 7.3 \times 10^{-4} M_\odot \text{ yr}^{-1}$. These values are of course rather uncertain, and but for instance we note that direct radio detections of a number of the stars in the Arches cluster by Lang, Goss & Rodríguez (2001) might suggest a broadly similar value for the total mass-loss rate from the cluster. However, in their simulation of the X-ray properties of the Arches cluster, Raga et al. (2001) assumed a somewhat larger integrated mass-loss rate (60 stars each with an individual mass-loss rate of $10^{-4} M_\odot \text{ yr}^{-1}$) but a lower mean terminal velocity (the wind of each star was assumed to have a terminal velocity of 1500 km s^{-1}). The calculations of Raga et al. (2001) did not include additional mass-loading and in the following section we shall see that to reproduce the X-ray properties of the Arches (and other) clusters we find that we do need to include mass-loading (or a lower η), which has a similar effect as an enhanced mass-loss rate and reduced terminal velocity.

Results from a 51 ksec ACIS-I *Chandra* observation of the Arches cluster have been presented by Yusef-Zadeh et al. (2002) and show three main emission regions probably associated with the Arches cluster (designated A1–A3 by Yusef-Zadeh et al. 2002). Two of these components are compact (A1 and A2) and one coincides with the core of the cluster (A1). The third component (A3) is more extended and part of it may be due to the cluster wind and part may be associated with fluorescent emission from a molecular cloud (C. Lang, private communication). Yusef-Zadeh et al. (2002) fitted the spectrum of this component with an additional line feature at 6.4 keV. The total X-ray luminosity (0.2 – 10 keV) from the 3 components is $5 \times 10^{35} \text{ erg s}^{-1}$, with component A1 being the most luminous. The spectra are fitted with a 2 component model, with $kT_1 \sim 0.8 \text{ keV}$ and $kT_2 \sim 6.4 \text{ keV}$ for the A1 component, and we shall use both these temperature values in the analysis, but only the overall luminosity. The two compact X-ray sources could be genuine point sources, associated with colliding stellar winds, or at least one of them could also be the unresolved core of a cluster wind.

¹ Available at <http://www.stsci.edu/science/starburst99>

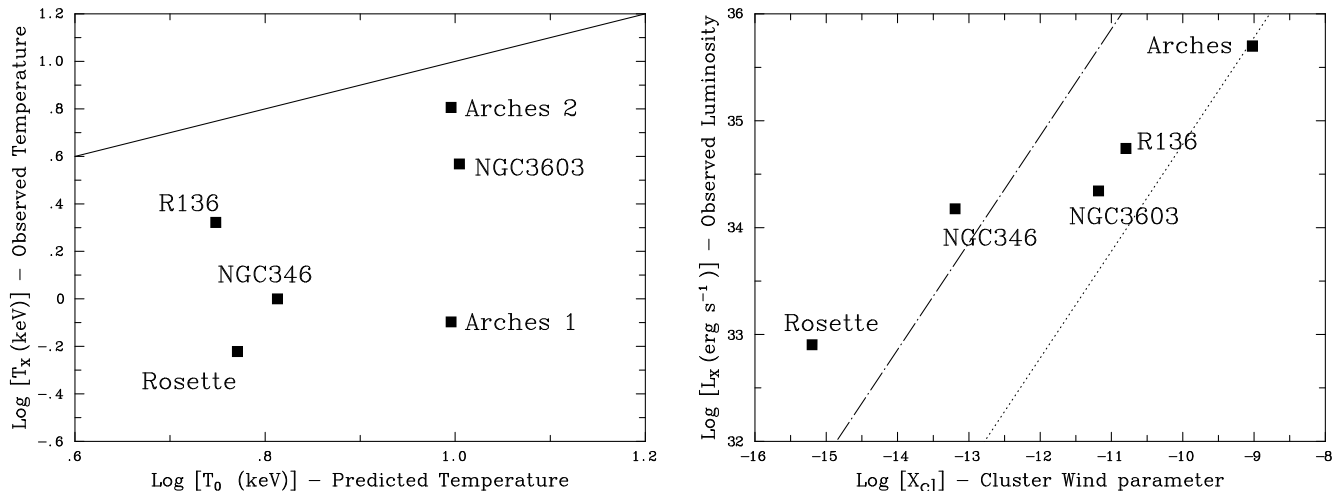


Figure 5. Left: The fitted X-ray temperature of the diffuse X-ray emission of the sample of star clusters versus the predicted X-ray temperature calculated from the model described in § 2. The solid line depicts equality, that is extremely efficient conversion of the kinetic energy in the winds of the component stars to thermal energy. Two values of observed temperature for the Arches cluster are plotted (see text for details). Right: The observed X-ray luminosity L_X versus the theoretical cluster wind parameter X_{cl} (eqn.10) for the sample clusters. Also plotted are two results from two models shown in Fig. 3, namely models with $\eta = 1$ and $\dot{M}_{cold} = \dot{M}_*$ (dotted line) and $\dot{M}_{cold} = 10\dot{M}_*$ (dot-dashed line).

4 RESULTS: COMPARISON OF THEORY AND OBSERVATION

From the theory developed in § 2 and the observational results that we have for the small number of clusters, presented in § 3 we can now make some comparisons. In Table 1 we summarise the theoretical and observational data for the sample clusters.

Fig. 5 (left panel) shows a plot of the observed X-ray temperatures from the *Chandra* observations versus the theoretically predicted wind temperatures for each cluster (specifically, values of T_0 are plotted, calculated using eqn. 9). It is clear that in all cases bar one the observed temperature is significantly lower than that the value predicted from the stellar population in the cluster. The exception is the case of the hotter component of the Arches cluster, where the discrepancy is much less. In the case of the Arches though, it should be remembered that the best-fit model to the X-ray spectrum had two components and the 2nd component is also plotted and is much more in line with the other clusters. In fact, the cooler component ($kT_1 \sim 0.8\text{keV}$) is more luminous than the hotter component and it may have been better to use that value. Also, R136 is rather more distant than the rest and the possibility of unresolved point sources contaminating the spectrum is more. If we were to ignore both the Arches cluster and R136 (of course, leaving only 3 data points) then a more coherent picture may be emerging of consistently lower observed temperatures. As has been noted before, such a reduction in observed temperature is a natural consequence of $\eta < 1$ or that significant mass-loading is occurring.

In § 2 the cluster wind model was also used to make predictions concerning the scaling of the cluster X-ray luminosity versus the cluster wind scaling parameter X_{cl} (see eqn. 10). The observed correlation between the measured L_X and X_{cl} is shown in the right panel of Fig. 5. The most notable feature is that compared to the standard model in Fig. 3 the clusters are all overluminous by over an order of magnitude. The second feature is that there does seem to be a clear correlation between L_X and X_{cl} , not necessarily linear, but apparently monotonic. For comparison, results from model calculations, already shown in Fig. 3, illustrate that the effects of mass-loading can roughly reproduce the X-ray luminosities of the cluster, with $\dot{M}_{cold} = 1 - 10\dot{M}_*$.

Similarly, very low values of η could yield the same result (with $\eta \sim 0.01$), though this would be in conflict with the observed temperatures.

It could be argued that this correlation is partly a consequence of the simple fact that we would expect more massive clusters to be more X-ray luminous, and undoubtedly the value of X_{cl} is most dependent on the total stellar mass-loss rate of the cluster (\dot{M}_*) and this will in turn scale with stellar mass. Larger clusters may also have larger populations of unresolved point sources making them appear more X-ray luminous. With the very limited sample we have it is difficult to go further than merely noting that there is a correlation between L_X and X_{cl} . The Rosette nebula appears to lie at a somewhat higher luminosity than its value of X_{cl} would imply. This could imply a larger comparative fraction of mass-loading as compared to the other clusters (see Fig. 3). The low observed temperature, as compared to the expected value, would tally with this.

In Fig. 3 we postulated that it may be possible to discriminate between the effects of a low thermalization efficiency and mass-loading by means of a stellar cluster X-ray luminosity temperature diagram. In Fig. 6 we show a plot of the observed values for the cluster sample. The model predicted that the luminosity and cluster temperature should be inversely correlated (though with different slopes depending on whether mass-loading or low thermalization efficiency was dominant). From Fig. 6 we can see clearly that the data suggest that X-ray temperature and luminosity are probably not well correlated.

5 SUMMARY AND CONCLUSIONS

In this paper we have presented a comparison between the theory of outflows from young star clusters in a cluster wind and X-ray observations of diffuse X-ray emission from these clusters. The high spatial resolution of *Chandra* is necessary to begin to disentangle the diffuse emission from point source emission. However, even with *Chandra* problems remain as to being sure that the diffuse emission is genuinely diffuse and associated with the clus-

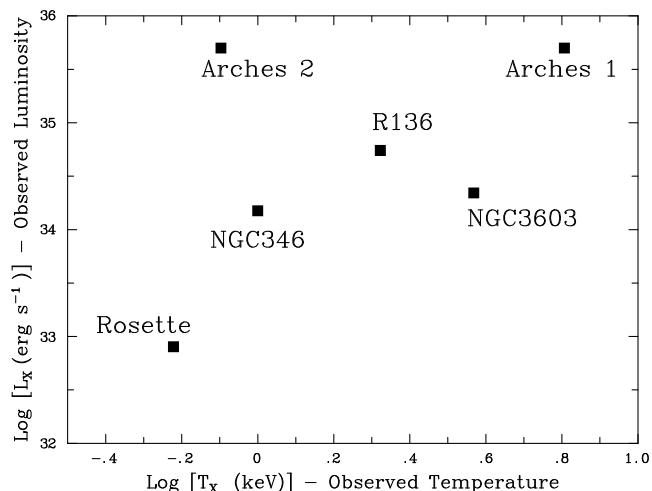


Figure 6. A stellar cluster X-ray luminosity-temperature diagram for the observed clusters, see text for more details. Note that the two values plotted for the Arches cluster correspond to the two fitted components (see text for details).

ter wind. The major problem remains the extremely small sample size. More observations will alleviate this problem to some extent, but the objects discussed here represent the best examples of such a cluster wind.

This analysis has thrown up some interesting results, the diffuse X-ray luminosity of the star clusters in the sample is correlated with the cluster wind scaling parameter $X_{cl} = \dot{M}_*^2 / (R_c \dot{V}_*)$ as predicted, but that the observed X-ray temperature is not well correlated with the predicted X-ray temperature (though a better correlation may be masked by the nature of the data). It is also clear that from these data it is very unclear as to what is going on in the clusters; is there a low thermalization efficiency or is mass-loading the dominant mechanism?

In this paper we have put together the results from several *Chandra* observations of nearby massive young star clusters to investigate the cluster wind. It is clear that many more observations will be required to take the study further, to make a clearer connection between the theory and observations of cluster winds. Such observations will be necessary to really understand the impact that star clusters will have on the interstellar medium of galaxies of all shapes and sizes.

REFERENCES

Aretxaga I., Benetti S., Terlevich R., Fabian A., Cappellaro E., Turatto M., della Valle M., 1999, *MNRAS*, 309, 343
 Blum R.D., Schaefer D., Pasquali A., Heydari-Malayeri M., Conti P.S., Schmutz W., 2001, *AJ*, 122, 1875
 Bradamante F., Matteucci F., D’Ercole A., 1998, *A&A*, 337, 338
 Brandner W., Grebel E.K., Chu Y.-H., Dottori H., Brandl B., Richling S., Yorke H.W., Points S.D., Zinnecker H., 2000, *AJ*, 119, 292
 Cantó J., Raga A., Rodríguez L., 2000, *ApJ*, 536, 896
 Chevalier R., Clegg A., 1985, *Nature*, 317, 44
 Chevalier R., Fransson C., 2001, *ApJ*, 558, L27
 Chu Y.-H., Mac Low M.-M., 1990, *ApJ*, 365, 510
 Cotera A.S., Erickson E.F., Colgan S.W.J., Simpson J.P., Allen D.A., Burton M. G., 1996, *ApJ*, 461, 750
 Crowther P., Dessart L., 1998, *MNRAS*, 296, 622
 Feigelson E.D., 2001, in Giacconi R., Serio R., Stella L., eds, ASP

Conf. Ser. 234, X-ray Astronomy 2000, Astron. Soc. Pac., San Francisco, p. 131
 Figer D.F., Kim S.S., Morris M., Serabyn E., Rich R.M., McLean I.S., 1999, *ApJ*, 525, 750
 Figer D.F., McLean I.S., Morris M., 1999, *ApJ*, 514, 202
 Gallagher J., Smith L., 1999, *MNRAS*, 304, 540
 Gregorio-Hetem J., Montmerle T., Casanova S., Feigelson E., 1998, *A&A*, 331, 193
 Hartquist T., Dyson J., Williams R., 1997, *ApJ*, 482, 182
 Holtzman J., Faber S., Shaya E., Lauer T., Grothe J., Hunter D., Baum W., Ewald S., Hester J., Light R., Lynds C., O’Neil E. J., Westphal J., 1992, *AJ*, 103, 691
 Howarth I.D., Prinja R.K., 1989, *ApJS*, 69, 527
 Johnson K., Leitherer C., Vacca W., Conti P., 2000, *AJ*, 120, 1273
 Kudritzki R.-P., Puls J., 2000, *ARA&A*, 38, 613
 Lang C.C., Goss W.M., Rodríguez L.F., 2001, *ApJL*, 551, L143
 Lehnert M., Heckman T., Weaver K., 1999, *ApJ*, 523, 575
 Leitherer C., Heckman T., 1995, *ApJS*, 96, 9
 Leitherer C., Schaefer D., Goldader J., Delgado R., Gonzalez R., Carmelle K., Denis F., de Mello D., Devost D., Heckman T., 1999, *ApJS*, 123, 3
 Massey P., Johnson K., DeGioia-Eastwood K., 1995, *ApJ*, 454, 151
 Massey P., Parker J., Garmany C., 1989, *AJ*, 98, 1305
 Mathewson D., Ford V., Visvanathan N., 1986, *AJ*, 301, 664
 Moffat A., Drissen L., Shara M., 1994, *ApJ*, 436, 183
 Moffat A.F.J., Corcoran M.F., Stevens I.R., Marchenko S.V., Skalkowski G., Mücke A., Koribalski B.S., Ptak A., Mushotzky R., Pittard, J.M., Pollock A.M.T., Brandner W., 2002, *ApJ*, 573, 191
 Montmerle T., Grosso N., Feigelson E.D., Townsley L., 2002, “New Visions of the X-ray Universe in the XMM-Newton and Chandra Era” (ed. F. Jensen et al.), ESA SP-488 (in press)
 Mücke A., Koribalski B., Moffat A., Corcoran M., Stevens I., 2002, *ApJ*, 571, 366
 Nazé Y., Hartwell J.M., Stevens I.R., Corcoran M.F., Chu Y.-H., Koenigsberger G., Moffat A.F.J., Niemela V.S., 2002a, *ApJ*, 580, 225
 Nazé Y., Hartwell J.M., Stevens I.R., Manfroid J., Marchenko S., Corcoran M.F., Moffat A.F.J., Skalkowski G., 2002b, *ApJ*, (submitted)
 Oey M.S., 1996, *ApJ*, 467, 666
 Origlia L., Leitherer C., Aloisi A., Greggio L., Tosi M., 2001, *AJ*, 122, 815
 Ozernoy L.M., Genzel R., Usov V.V., 1997, *MNRAS*, 288, 237
 Portegies-Zwart S., 2001, In: Dynamics of Star Clusters and the Milky Way, ASP Conference Series, Vol. 228. Eds: S. Deiters, B. Fuchs, R. Spurzem, A. Just, and R. Wielen. San Francisco, p.131
 Raga A.C., Velázquez P.F., Cantó J., Masciadri, E. Rodríguez L.F., 2001, *ApJ*, 559, L33
 Recchi S., Matteucci F., D’Ercole A., 2001, *MNRAS*, 322, 800
 Serabyn E., Shupe D., Figer D., 1998, *Nature*, 394, 448
 Strickland D., Heckman T., Weaver K., Hoopes C., Dahlem M., 2002, *ApJ*, 568, 689
 Strickland D., Stevens I., 2000, *MNRAS*, 314, 511
 Whitmore B., 2000, astro-ph/0012546
 Whitmore B., Schweizer F., 1995, *AJ*, 109, 960
 Yusef-Zadeh F., Law C., Wardle M., Wang Q., Fruscione A., Lang C., Cotera A., 2002, *ApJ*, 570, 665